Direct Modular Multilevel Converter With Six Branches for Flexible Distribution Networks

Javier Pereda, *Member, IEEE*, and Tim C. Green, *Senior Member, IEEE*

***Abstract*—This paper presents a complete analysis of a direct ac-to-ac modular multilevel converter (direct MMC) applied in medium-voltage distribution networks through the soft-open-point concept. The direct MMC is capable of bidirectional power flow between two feeders at any power factor, even when the feeders have different nominal voltages and operate with a phase-shift angle or unbalanced voltages. The converter has six branches, each one composed of full H-bridges cells connected in series to generate a multilevel voltage waveform, to share the blocking voltage of the power switches and to have fault-tolerant operation. This paper presents a suitable control scheme and provides a discussion about the capabilities and limitations of the converter, the capacitor voltage balance control, the efficiency, and the power-loss mitigation at various operation points. Simulation results and power-loss calculations are presented for a three-phase 11-kV 16-MVA direct MMC with 10 H-bridge cells per branch. The direct MMC is simulated in a distribution network to demonstrate the features of the converter and control under various operation conditions, including grid faults.**

***Index Terms*—AC-AC power converters, direct power conversion, grid-connected converters, matrix modular multilevel converters, power-flow controller, soft open point (SOPs).**

I. Introduction

DISTRIBUTION networks will need to become more flexible to accommodate an increase in distributed generation (DG) as well as a higher peak demand produced by the charging of electric vehicles (EVs). The integration of these technologies brings serious problems for the grid as unbalance voltages, higher peak and fault currents, unnecessary protection activation, and voltage drop or rise in adjacent feeders. The existing networks are becoming ineffective to solve these problems because the only control is a transformer tap-changer at 33/11 kV substations and there is no automatic control at 11/0.4 kV, where the DG and EVs are connected, so it is not possible to cope with different feeders at the same time [1]. Therefore, the modernization of the 11 kV and 400 V distribution network is critical to integrate non-conventional renewable energies, DG and EVs without losing reliability, power quality and efficiency. Possible solutions are to engage the management of DG and EVs connections [2], add mesh connection to radial feeders [3], use active compensation or energy storage systems [4], and implement soft-open-points (SOPs) to obtain a soft meshed distribution network with power-flow-control [5], [6].

Active compensation has been widely used in transmission (FACTS) and can be also applied to distribution, but it is important to notice the specific requirement of the distribution network [7]. The static synchronous compensator (STATCOM) is not able to interconnect two feeders and only controls the reactive power-flow; the static synchronous series capacitor (SSSC) has a limited control of the real and reactive power-flow, is not able to block flow of fault currents and requires some special protection; the unified power flow controller (UPFC) has a good power-flow-control but has the same problems as the SSSC with the fault isolation; and the back-to-back (B2B) converter is the most flexible and powerful solution for power-flow-control between two feeders and is able to manage the current fault, but it requires two fully-rated power converters [8], [9]. The application of power converters on distribution networks is very restricted to cost, footprint, reliability and power losses. Therefore, the ac-to-ac (direct) power converters seems to be an attractive alternative to the back-to-back converter, but has not been extensively analysed for this propose.

Distribution network operators (DNO) favour the connection of DGs at higher voltage feeders (33 or 132 kV in U.K.) to reduce the negative impact, but DG owners prefer a connection at lower voltage (11 kV or 400 V in U.K.) to reduce cost. Therefore, the application of power converters as SOPs in 11 kV feeders seems to be a good option to solve the problems in the distribution network [8].

Several power converter topologies can be used for power-flow-control in 11 kV feeders, as the back-to-back two-level inverter, the back-to-back modular multilevel converter (MMC) or the Direct MMC. The conventional two-level inverter is the most mature technology but requires IGBTs connected in series, has high switching power losses, generates a high Total Harmonic Distortion (THD), and does not have fault tolerant operation [10]. The MMC is a promising technology for HVDC transmission, presents high efficiency, fault tolerant operation and low THD, but it has a big footprint, high cost and has not been applied in distribution networks, so a more in-depth study is required [11]–[15]. On the other hand, the direct MMC is an immature technology that has been usually proposed for low-speed motor drives and discarded for connection to synchronous systems due to instabilities presented at synchronous operation [16]–[20]. However, the ac-to-ac power conversion of the direct

Manuscript received September 11, 2015; revised December 14, 2015; accepted January 13, 2016. Date of publication March 03, 2016; date of current version July 21, 2016. This work was supported in part by the Reconfigurable Distribution Networks project under ESPRC Grant EP/K036327/1 and in part by the CONICYT through FONDECYT 11130513. Paper no. TPWRD-01286-2015.

J. Pereda is with the Department of Electrical and Electronics Engineering, Imperial College, London SW7 2AZ, U.K. and also with the Department of Electrical Engineering, Pontificia Universidad Católica de Chile, Santiago 7820436, Chile (e-mail: jperedat@ic.ac.uk).

T.C. Green is with the Department of Electrical and Electronics Engineering, Imperial College, London SW7 2AZ, U.K. (e-mail: t.green@ic.ac.uk).

Color versions of one or more of the figures in this paper are available online at http//ieeexplore.ieee.org.

Digital Object Identifier 10.1109/TPWRD.2016.2521262

This work is licensed under a Creative Commons Attribution 3.0 License. For more information, see http://creativecommons.org/licenses/by/3.0/

MMC is attractive for distribution networks and keeps some advantages from the conventional MMC as the high modularity, fault tolerant operation and low THD. Therefore, the direct MMC seems to be a possible solution to reduce cost, footprint and power losses compared to back-to-back power converters.

A direct ac-to-ac MMC was proposed in 2011 using only six branches instead of nine [21], [22]. This converter is called hexverter or hex-converter and is attractive for connecting two three-phase systems due to its simplicity. However, it presents similar instabilities as the direct MMC under synchronous operation, so has been focused in low speed applications as wind turbines. Nevertheless, the converter should work stably under such synchronous operation provided that phase connections are arranged to ensure that there is an AC voltage across each converter branch at any operation point.

This paper is focused on the application and analysis of a 16 MVA direct MMC to control the power-flow between two 11 kV feeders using only six branches, each composed of 10 H-bridge cells. The control of the direct MMC is based on one current controller per branch and is capable of operating the converter in the four PQ quadrants, balancing the capacitor voltage of each cell and blocking the current under a short circuit fault. The control is also capable of operating the converter under unbalanced voltage and even when the feeders operate at different nominal voltages (e.g., 11 kV–6.6 kV). The currents generated by the converter present a low THD and no filter is required. The power losses are calculated and compared for various point of operation, showing a high efficiency even at low power operation. Moreover, also some limitations and drawbacks of the converter are presented.

II. Direct Modular Multilevel Converter (MMC)

Fig. 1 illustrates two synchronized three-phase systems (*abc* and *ABC*) connected through power converters that control the power flow between the two systems. These systems represent feeders of the distribution network, so they have the same frequency and usually the same nominal voltage and phase. However, in distribution network it is common that feeders present unbalance voltages and in some specific cases a phase shift if they are connected to different transformer configurations (feeders from different substations).

A. Topology

The converter shown in Fig. 1(a) is a B2B-MMC with half H-bridges and the converter in Fig. 1(b) is a direct MMC with full H-bridges and only six arms. Both converters are capable of isolating current faults in any feeder and have fault tolerant operation due to the modularity. The direct MMC has no dc-link and has the same number of semiconductors but half the number of capacitors and inductors than the B2B-MMC. However, a more exhaustive analysis of both topologies must be made to compare the control flexibility, voltage blocking and current required of each semiconductor, capacitor and inductor sizes, and power losses.

It is mandatory to guarantee an AC voltage on each arm at all times to obtain a stable operation of the direct MMC

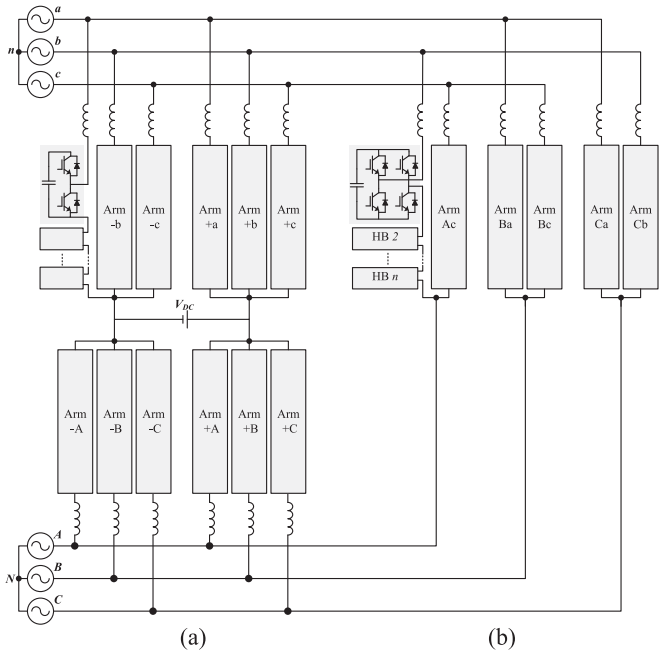


Fig. 1. Modular multilevel converters as soft-open-point. (a) Back-to-Back MMC. (b) Direct MMC (Hex-converter).

working at synchronous operation (50 Hz). For instance, Fig. 1(b) shows converter arms connecting phase *A* of the bottom feeder to phases *b* and *c* of top feeder.

The ac-to-ac topology of the direct MMC converter implies that the currents between the the two feeders are not independent, as shown in Fig. 2 and (1). This entail a coupled reactive power between the two feeders, which means the converter inject or consume exactly the same amount of reactive power in both feeders. Moreover, the coupled currents carry limitations if the feeders have unbalanced voltages, because the converter can provide unbalance compensation only to one feeder at a time, neglecting the unbalance compensation for the other one. These drawbacks will be shown in simulations and discussed in the last sections.

B. Basic Operation

The direct MMC operation is based on a current controller per each arm to obtain the line reference current, as shown in (1) and Fig. 2. The arm currents i_{Ab} and i_{Ac} operate in concert to generate i_A^* with the restriction to be at 90° from the respective voltages v_{Ab} and v_{Ac}. Therefore, only their magnitudes change according to the reference line current i_A^*.

$$i_A^* = i_{\mathrm{Ab}} + i_{\mathrm{Ac}} \tag{1}$$

The idea is to operate each arm as a reactive current generator to achieve energy balance of the capacitors. Then, any reference line current can be obtained from the vector sum of the two reactive currents. However, a small active current must be introduced to adjust the energy balance error of the capacitors. Therefore, a PI controller is introduced on each arm to inject active current if the capacitors are overcharged or to consume active current

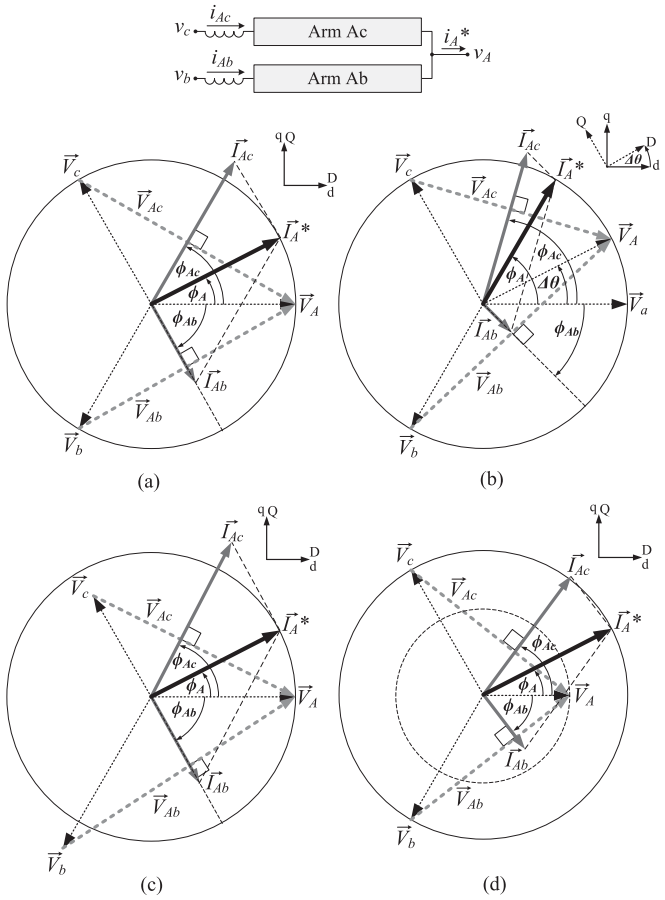


Fig. 2. Phasor diagram of the currents and voltages of arm Ab and Ac under different operation case scenarios. (a) Both system synchronised and balanced. (b) Phase shift ($\Delta\theta = 30^\circ$) between the two systems. (c) System *abc* with unbalance voltages. (d) Systems of different voltages (11 kV and 6.6 kV).

if the capacitors are undercharged. This PI controller manages the total energy of the capacitors on an arm, so it is necessary to add a second balance control to manage the energy of each capacitor of an arm, which is done on the modulation through a proportional controller [23].

Fig. 2(b) illustrates the operation of the direct MMC when the feeders have a phase shift (e.g., $\Delta\theta = 30^\circ$). Fig. 2(c) shows the operation when the feeder *abc* has unbalanced voltages and Fig. 2(d) shows the operation when the systems have different nominal voltages (e.g., 11 kV – 6.6 kV). The proposed control therefore can operate between feeders with different nominal voltages, phase-shift angles and unbalance voltages.

C. Power Rating of the Converter

The voltage of each arm is equal to the voltage between the lines of the two feeders as shown in Fig. 2. Therefore, the arm voltage depends on the nominal voltage of each feeder, the phase shift between them and the interconnection chosen among the lines. The voltage of each arm can be calculated using trigonometry as shown in (9) and it will be different for each arm if the feeders have a phase shift as illustrated in Fig. 2(b). Anyway, the worst case scenario is when the phase shift is $\Delta\theta = 60^\circ$ because one arm blocks twice the line-to-ground voltage of the feeder while the other arm only blocks half (e.g., 18 $\mathrm{kV_{peak}}$ and 9 $\mathrm{kV_{peak}}$ for feeders of 11 kV). Therefore, this maximum blocking voltage is similar to the B2B-MMC but only in half of the arms. On the other hand, the direct MMC has to block less voltage than the B2B-MMC if the feeders have different voltages because the B2B dc-link voltage must be rated for the feeder with higher voltage.

The current of the IGBTs is equal to the arm current and can be calculated using (6) and (7). This current depends on the nominal voltage of each feeder and can be different for each arm according to the phase shift between feeders and the power factor of operation, ranging from 0.0 pu to 1.15 pu of the feeder line current. As an example, assuming $\Delta\theta = 0^\circ$, the arm current of both arms is 1.0 pu for $\phi = 0^\circ$ $(\mathrm{PF} = 0)$; 1.15 pu $\left(2/\sqrt{3}\right)$ and 0.58 pu $\left(1/\sqrt{3}\right)$ for $\phi = 30^\circ$ $(\mathrm{PF} = 0.87)$; and 1.0 pu and 0.0 pu for $\phi = 60^\circ$ $(\mathrm{PF} = 0.5)$.

III. Control of the Direct MMC

Fig. 3 illustrates the control block diagram for the leg A of the converter (arm Ab and Ac). The first step is to calculate the positive sequence angles and voltages of both systems through an enhanced phase-locked loop (EPPL) system [24]. The angle of the system *abc* (θ_v) is used as reference for the entire control, and the angle of system *ABC* (θ_V) is required to calculate the phase shift $\Delta\theta$ between the two systems. Then, the reference current i_A^* is calculated by the power controller block using the reference active and reactive power P and Q, and the voltages v_D and v_Q as is presented in (2) and (3).

$$i_D^* = \frac{P^* \cdot v_D + Q^* \cdot v_Q}{v_D^2 + v_Q^2} \tag{2}$$

$$i_Q^* = \frac{P^* \cdot v_Q - Q^* \cdot v_D}{v_D^2 + v_Q^2} \tag{3}$$

The reference current i_A^* is obtained directly from the current i_{DQ}^*, as shown in (4) and (5). The current angle ϕ_A^* is obtained adding the phase shift $(\Delta\theta)$ because the system dq is used as reference.

$$\left|\vec{I}_A^*\right| = \sqrt{\frac{2}{3}}\left|\vec{I}_{\mathrm{dq}}^*\right| = \sqrt{\frac{2}{3}}\left|\vec{I}_{\mathrm{dq}}^*\right| \tag{4}$$

$$\phi_A^* = \phi_{\mathrm{dq}}^* = \phi_{\mathrm{dq}}^* + \Delta\theta \tag{5}$$

Then, the current magnitude calculator block of leg A uses the line reference vector $\vec{I}_A^*$ and the arm current angles ϕ_{Ab}^* and ϕ_{Ac}^* to calculate the magnitudes of $\vec{I}_{\mathrm{Ac}}^*$ and $\vec{I}_{\mathrm{Ab}}^*$ through (6) and (7). These equations are a simple geometric relation of the currents vectors $\vec{I}_A$, $\vec{I}_{\mathrm{Ab}}$ and $\vec{I}_{\mathrm{Ac}}$ as shown in Fig. 2.

$$I_{\mathrm{Ac}}^* = I_A^* \frac{\sin(\phi_A^*) - \cos(\phi_A^*) \cdot \tan(\phi_{\mathrm{Ab}}^*)}{\sin(\phi_{\mathrm{Ac}}^*) - \cos(\phi_{\mathrm{Ac}}^*) \cdot \tan(\phi_{\mathrm{Ab}}^*)} \tag{6}$$

$$I_{\mathrm{Ab}}^* = \frac{I_A^* \cdot \cos(\phi_A^*) - I_{\mathrm{Ac}}^* \cdot \cos(\phi_{\mathrm{Ac}}^*)}{\cos(\phi_{\mathrm{Ab}}^*)} \tag{7}$$

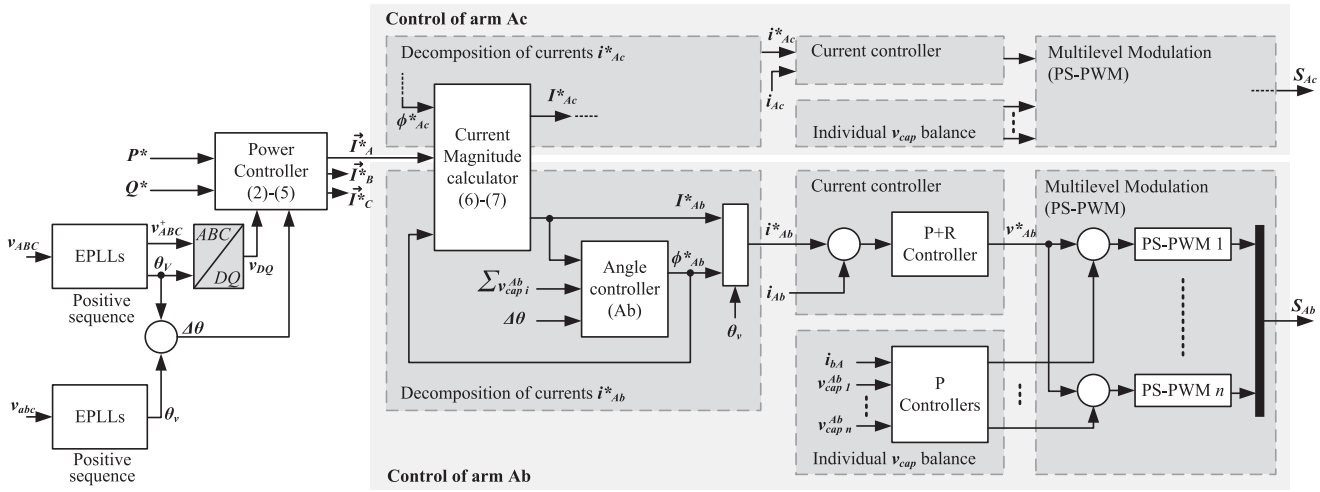


Fig. 3. Control Block diagram of leg A of the direct MMC.

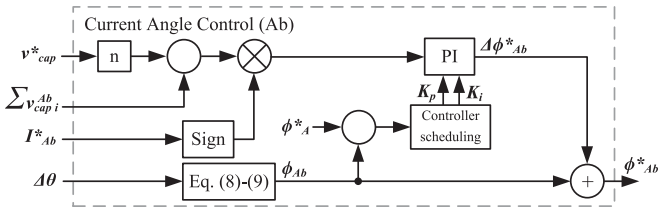


Fig. 4. Controller block of the current angle ϕ^*_{Ab}.

According to the basic operation theory, the angle ϕ^*_{Ab} and ϕ^*_{Ac} should be at 90° of the respective voltage of each arm to keep the capacitor voltages (each arm generate a pure reactive current). However, in practice these angles must be slightly corrected by the angle controller to compensate any error.

Fig. 4 shows the angle controller of arm Ab. The bottom block is a feed-forward control which calculates the theoretical reference angle ϕ_{Ab} using (8) and (9) to ensure the current $\vec{I}^*_{\mathrm{Ab}}$ operates at 90° respect to the arm voltage $\vec{V}_{\mathrm{Ab}}$, so the phase-shift angle between the two systems $\Delta\theta$ and their nominal voltages V_{abc} and V_{ABC} are taken into account.

$$\phi_{\mathrm{Ab}} = -\frac{\pi}{6} - \mathrm{asin}\left(\frac{V_{\mathrm{ABC}} \cdot \sin\left(\frac{2\pi}{3} + \Delta\theta\right)}{V_{\mathrm{Ab}}}\right) \tag{8}$$

$$V_{\mathrm{Ab}} = \sqrt{V^2_{\mathrm{abc}} + V^2_{\mathrm{ABC}} - 2V_{\mathrm{abc}}V_{\mathrm{ABC}}\cos\left(\frac{2\pi}{3} + \Delta\theta\right)} \tag{9}$$

Then, the reference angle ϕ_{Ab} is deviated slightly by adding a correction angle $\Delta\phi^*_{\mathrm{Ab}}$ that is generated by a PI controller that uses the capacitor voltages error. This error is multiplied by the sign of I^*_{Ab} calculated in (7), which reflects if $\vec{I}_{\mathrm{Ab}}$ is leading or lagging $\vec{V}_{\mathrm{Ab}}$, to inject/deliver power to/from the arm when the capacitors are undercharged/overcharged. The PI controller is also responsible to correct the current angle ϕ^*_{Ab} when one or both systems have unbalanced voltages.

The PI controller uses online gain scheduling to improve the performance and control stability at different points of operation. The gains change according to the percentage contribution of the arm to the reference current of the line. The contribution of the two arms in one leg is complementary and it is a function of the current angle ϕ. The gain scheduling is essential to ensure stability when the contribution of one arm is considerably high such as when the reference angle ϕ matches with the angle of one arm (e.g., converter operating with $\Delta\theta = 0°$ and power factor of 0.5). In this case one arm of the converter leg provides nearly all the current and the other one operates at very low current amplitude but with a highly variable angle, which might generate instabilities if the controller is not adapted. This gain scheduling of the PI controller also reduces the switching power losses and current distortion because it generates a smooth reference for the PS-PWM modulation.

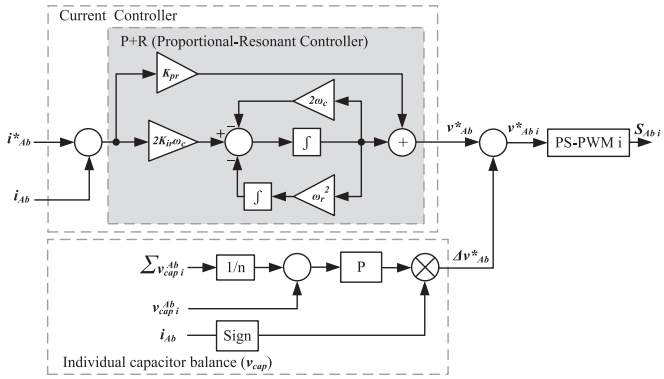


Fig. 5. Proportional-Resonant current controller, individual capacitor voltage balance controller and multilevel modulation for cell i.

Fig. 5 shows the current controller of i^*_{Ab}. A proportional-resonant controller was chosen instead of a PI controller because it has a better performance for AC signals, eliminating the steady error and increasing the response time. The current error is introduced in the proportional-resonant controller with a resonant frequency ω_r and a cut-off frequency ω_c to calculates the reference voltage of the arm v^*_{Ab}. This voltage is used as the reference of the phase-shift-PWM (PS-PWM) of each cell

TABLE I
PARAMETERS OF THE SYSTEM

Description	Parameter	Value
Grid nominal voltage	$V_{\mathrm{line-line}}$	11 kV
Grid nominal frequency	f	50 Hz
N° of HB per arm	n	10
HB capacitors size	C	6 mF
HB capacitors voltage	V_C	1.8 kV
Total energy in capacitors (x60)	E_{cap}	583 kJ
Arm inductor size	L	4.8 mH (0.2 pu)
Arm inductor resistance	r_L	15.8 mΩ (Q = 100)
Switching frequency	f_s	400 Hz
IGBT 5SNA1200E330100	–	3.3 kV & 1.2 kA
Converter power	S	16 MVA
Proportional gain of PI (range)	K_p	$[7\text{–}1400] \times 10e^{-8}$
Integral gain of PI (range)	K_i	$[4.4 - 35] \times 10e^{-4}$
Proportional gain of P+R	K_{pr}	$5{\times}10e^{-3}$
Resonant gain of P+R	K_{ir}	5
Resonant frequency of P+R	ω_r	$2\pi \cdot 50$
Cut-off frequency of P+R	ω_c	$2\pi \cdot 0.1$
Proportional gain of P	K	$1 \times 10e^{-3}$

(H-bridge). However, the voltage reference v^*_{Ab} is adjusted slightly for each cell by the individual capacitor controller to balance the capacitor voltage individually. The reference voltage deviation Δv^*_{Ab} is calculated by a proportional controller that uses the error of the capacitor voltage of the cell i respect to the capacitor voltage average on the respective arm. As the capacitor voltage average is used, the sum of all voltage deviation of one arm is equal to zero, which means no voltage distortion is generated in the arm. It is important to notice that the voltage deviation is multiplied for the current sign of the arm to inject or consume the correct amount of active power. Finally, the voltage v^*_{Abi} is introduced as the reference of the PS-PWM of cell i to obtain the switching signals S_{Ab}.

IV. SIMULATION RESULTS

A simulation model of the direct MMC with the proposed control has been realised in Matlab/Simulink using the SimPowerSystem toolbox to validate the control performance and to calculate the power losses at various operation points and conditions. Table I summarizes the parameters of the 16 MVA direct MMC used as a power-flow controller between two three-phase feeders of 11 kV and 50 Hz. The nominal voltage of each arm was selected to allow operation at the worst condition, which is when the systems have a phase shift $\Delta\theta = 60^\circ$, causing some arms to have to provide a maximum voltage of 18 kV between lines, as is calculated in (10).

$$V^{\mathrm{peak}}_{\mathrm{max}} = 2 \cdot \sqrt{2} \cdot \frac{11\,\mathrm{kV}}{\sqrt{3}} = 18\,\mathrm{kV} \tag{10}$$

The converter therefore uses 10 cells (full H-bridges) per arm with capacitors of 6 mF at 1.8 kV and uses IGBTs of 3.3 kV and 1.2 kA (such as ABB part 5SNA1200E330100). The capacitance was selected to obtain a maximum voltage ripple of $\pm 10\%$ in each capacitor. The switching frequency of each cell was fixed at 400 Hz because at this frequency a good trade-off is achieved between the switching power losses and the THD of current. The direct MMC generates a high number of voltage states (e.g., 21) at any operation point, so no high-order filters are required in the converter or feeders, only one inductor of 5 mH per arm. The converter is connected directly to the grid without transformers to reduce cost, footprint and power losses. The gains of the controllers were tuned manually and the gains of the PI controller are scheduled according to the current angle of the line and the respective arm through a nonlinear function implemented in a look-up table.

TABLE II
POWER LOSSES AND EFFICIENCY ($\Delta\theta = 0^\circ, T_{\mathrm{vj}} = 25^\circ$ C)

Total Power	Power Factor.	Efficiency	Conduction Losses	Switching Losses
16 MVA	1.0	97.54%	219.8 kW	173.4 kW
16 MVA	0.7	97.53%	150.6 kW	128.9 kW
8 MVA	1.0	97.62%	87.0 kW	103.7 kW
1.6 MVA	1.0	96.63%	11.8 kW	42.1 kW

The following simulations were obtained at various operation points and conditions, including the worst case scenario for the control. First, the power losses are calculated for four different power ratings. Then, several simulations are presented in five situations: (i) operation of the converter under ideal conditions; (ii) under a fault (three-phase short circuit) in one feeder; (iii) under dynamic power operation; (iv) under the worst case conditions; and (v) when the two feeders have different nominal voltages (11 kV – 6.6 kV).

A. Power Losses

The power losses were calculated using the curves provided by the manufacturer of the IGBTs and according to the standard BS EN 62751:2014 presented in [25] and [26]. The following power losses were taken into account: (i) IGBT conduction losses; (ii) IGBT turn-on and turn-off switching losses; (iii) diode reverse recovery losses; and (v) diode conduction losses. These power losses represent the main power loss of the converter and all the losses in the power electronics because snubbers are not required. Other power losses, such as the capacitor losses, the valve electronic power consumption and other valve conduction losses were not calculates because are very lower in comparison [27] and depend on detailed considerations in the design and implementation.

Table II shows the power losses and the efficiency of the power converter for four different operation points. The direct MMC has an efficiency of 97.54% at nominal power and unitary power factor. The conduction losses represent 56% and the switching losses 44%. The conduction losses decrease with the power of the converter, while the switching losses become more relevant. As an example, the efficiency at half nominal power is higher (97.62%) than at nominal power and the conduction losses represent 46% of the total. However, the efficiency at very low power (1.6 MVA) decreases to 96.63% due to the switching losses which represent 78% of the total. On the other hand, the efficiency of the converter at nominal power (16 MVA) is similar working with a power factor equal to 0.7 than with 1, even

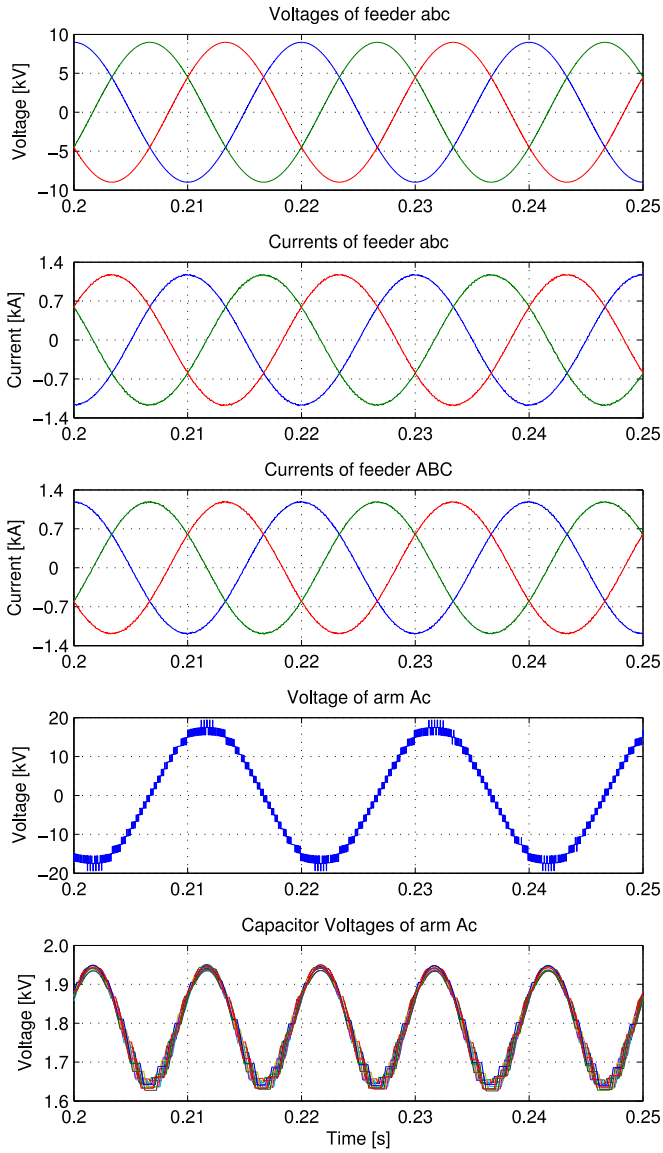


Fig. 6. Simulation of the direct MMC under ideal conditions.

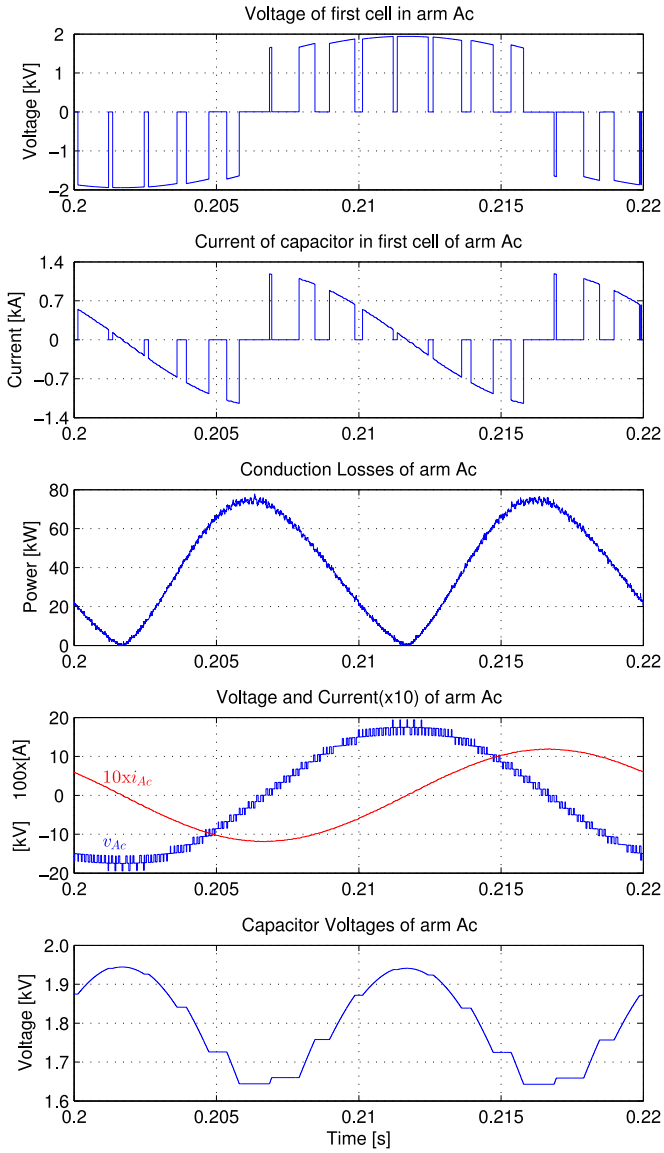


Fig. 7. Simulation in arm Ac under ideal conditions.

when the current magnitude is the same in the feeder line. This situation is due to one arm conducts most of the line current while the other one conducts only a very small current, as was explained in Section II.C. In summary, the efficiency of the converter increases as the active power decreases until the switching losses becomes too relevant, which happens at very low power. Further, reactive power generation does not necessarily mean higher losses.

The control principle of the converter reduces the conduction losses because the current and the voltage of each arm are always at 90°, as shown in Fig. 6 and 7. Under this conditions, most of the IGBTs conduct when the collector current is low and only one IGBT per cell conducts when the collector current reach me maximum value, so most of the current is carried by the diodes. Fig. 7 illustrates the conduction power losses in one arm, which reaches the maximum value when the cells are at zero voltage.

B. Performance Under Ideal Conditions

The direct MMC was simulated at nominal power (16 MVA) operating with unity power factor (pure active power-flow) and without phase shift between the two feeders ($\Delta\theta = 0°$) and balanced voltages. Fig. 6 shows the simulation results of the feeder voltages, the feeder currents, the voltage of arm Ac and the capacitor voltages of arm Ac. The current of feeder *abc* is at 180° from the grid voltage and from the current of feeder *ABC*. The THD of the current of both feeders is 0.9%. The voltage of the arm Ac has 21 levels generated by the 10 full H-bridges connected in series and it has a peak voltage of 19.5 kV, higher than the selected nominal peak voltage of 18 kV due to the capacitors being overcharged when the arm voltage reaches the peak. The capacitor voltages of arm Ac are balanced and have a maximum ripple lower than ±10%.

Fig. 7 shows the output voltage of one cell, the current and voltage of the cell capacitor, and the conduction power losses,

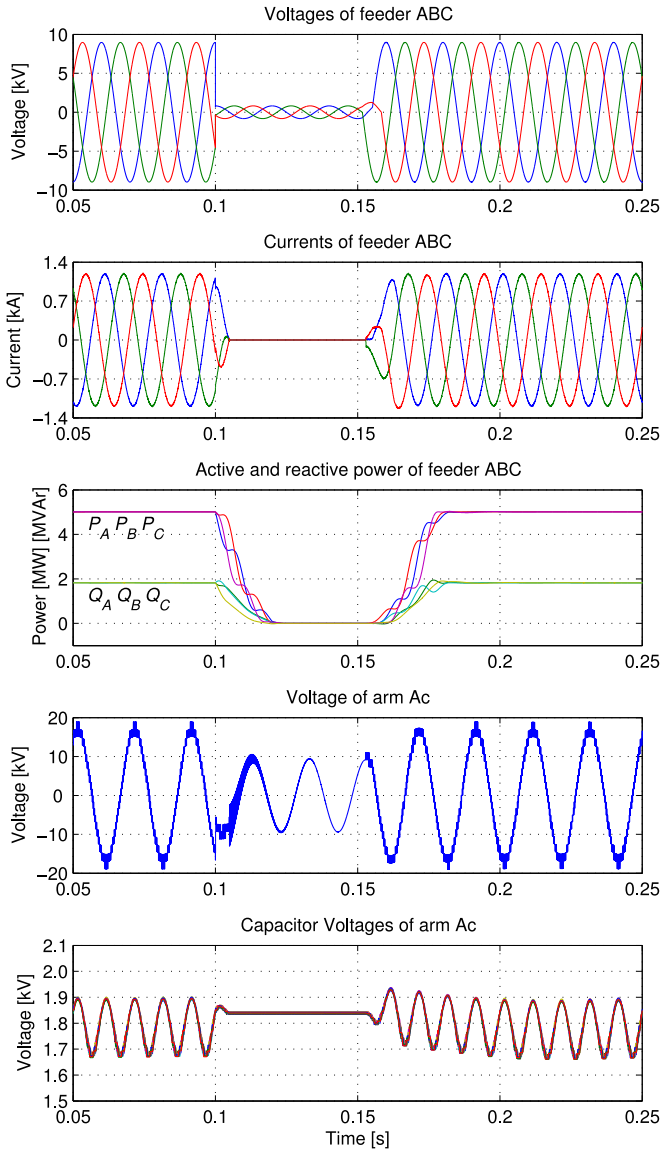


Fig. 8. Simulation of the direct MMC under fault (three-phase short circuit).

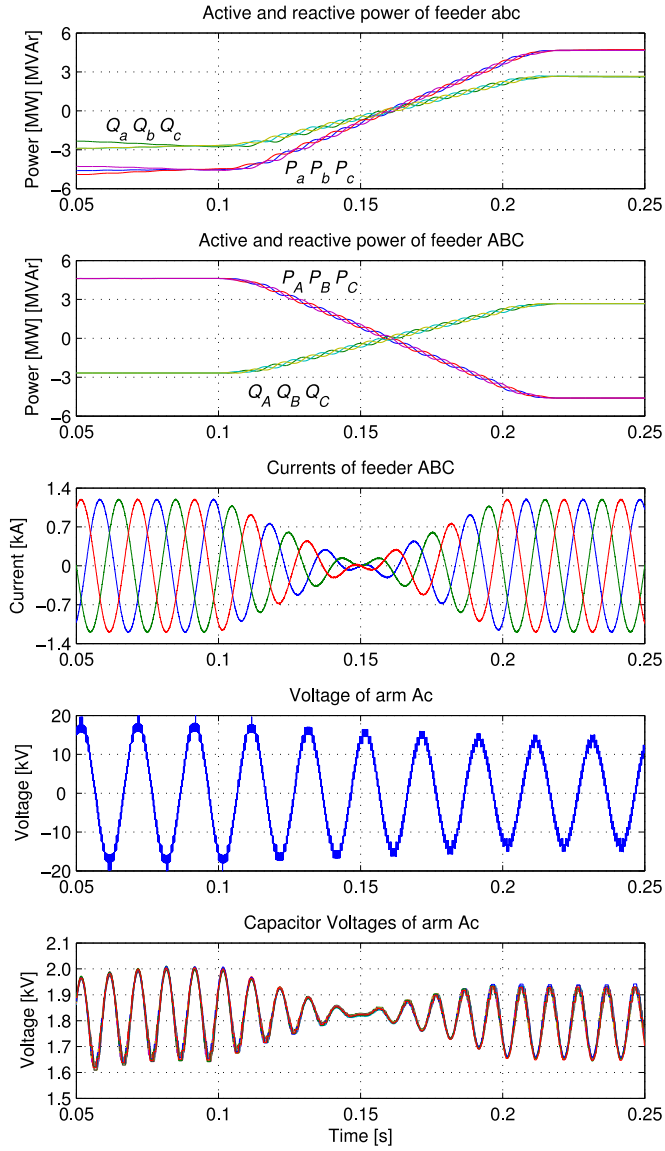


Fig. 9. Simulation results under dynamic operation.

voltage and current of the respective arm. The maximum conduction power losses are generated where the arm voltage is zero, which helps to reduce the losses. The capacitor voltage ripples at a frequency of twice fundamental frequency which is normal for single-phase ac element. The capacitor voltage increases when the current and voltage have different signs and it decreases when they have the same sign, conditions which happen twice per fundamental cycle.

C. AC Fault Blocking Capability

The direct MMC was simulated under a three-phase fault consisting of a short circuit between each line of feeder *ABC* and ground between 0.1 and 1.15 seconds (Fig. 8). The voltages are balanced, without phase shift and with a lagging $\mathrm{PF} = 0.94$. The control detects the fault and activates the fault mode operation to block the fault current. Therefore, the converter decreases its current to zero until the fault is cleared. The current is decreased or increased in a controlled manner through a rate limiter to prevent an excessive peak of voltage in the arm inductors due to a high $\mathrm{di/dt}$. After the current has been controlled to zero all the IGBTs are turned off. While the converter is turned off during the fault, the voltage of each arm is equal to the line-to-ground voltage of feeder *ABC*. The power flow between the two feeders is zero during the fault, and it is quickly restored when the fault is cleared. Finally, the capacitor voltages do not require any control during the fault because no current flows through the converter.

D. Performance Under Dynamic Power Operation

The direct MMC was simulated with a dynamic power operation, which consists of a reversal of power over a period of 0.1 seconds while keeping a leading $\mathrm{PF} = 0.87$. Fig. 9 shows

the simulations assuming balanced voltages and no phase shift. The active and reactive power are controlled with high accuracy at all times. It is important to note that the reactive power is coupled between the two feeders due to the ac-to-ac topology and control characteristics, which mean that both sides of the converter generate or consume exactly the same amount of reactive power. This situation is due to the coupling of the currents and it is inherent to the topology and control principle of the converter, which was explained in Section II. The currents of both feeders have a high quality during the reversal of power. The arm voltage also maintains a high quality, changing slightly during the reversal of power. The capacitor voltages are controlled without problems and their voltage ripple is related to the current magnitude.

E. Performance Under the Worst Case Conditions

The direct MMC was simulated at nominal power (16 MVA) operating with a leading power factor equal to 0.7, a phase shift between feeders ($\Delta\theta = 30°$) and unbalanced voltages of 2.9%, as shown in Fig. 10. According to the British standard, the voltage unbalance limit for systems with a nominal voltage below 33 kV is 2% for less than one minute and 1.3% for long term [28]. The chosen power factor, in conjunction with this phase shift, represents the worst case scenario for control stability because the reference line current vector overlaps the vector current of one arm, therefore, the line current is provided almost entirely by one converter arm while the other arm works at very low power but with a highly variable current angle to correct any error. Nonetheless, the capacitor voltages are controlled within reasonable limits and the entire control remains stable due to the online gain scheduling of the PI controller of Fig. 4. In this case, the controller scheduling reduces K_p for the PI controller in both arms of one leg, while it increases K_i for one arm and decreases it for the other one.

The currents of feeder *ABC* are balanced because the power controller generates the reference currents of this feeder using a three-phase reference of power and the positive sequence voltages of the feeder. On the other hand, the currents of feeder *abc* are unbalanced because they are generated according to the reference currents of the other feeder, so any unbalance voltages in the grid generate unbalance currents in this feeder. This happens because the currents between the two systems are coupled, as was discussed in Section II.

The active and reactive power of both feeders are unbalanced. However, balancing of power can be achieved in feeder *ABC* by replacing the three-phase power controller block for three single-phase power controllers. Nevertheless, these controllers can balance the power in only one feeder, because the current coupling does not allow independent current control in the two feeders simultaneously.

F. Feeders at Different Nominal Voltages (11 kV and 6.6 kV)

The direct MMC was simulated between one feeder of 11 kV and other of 6.6 kV, operating with unity power factor, balanced voltages and without phase shift between the two feeders ($\Delta\theta = 0°$), as shown in Fig. 2(d). The power rating of

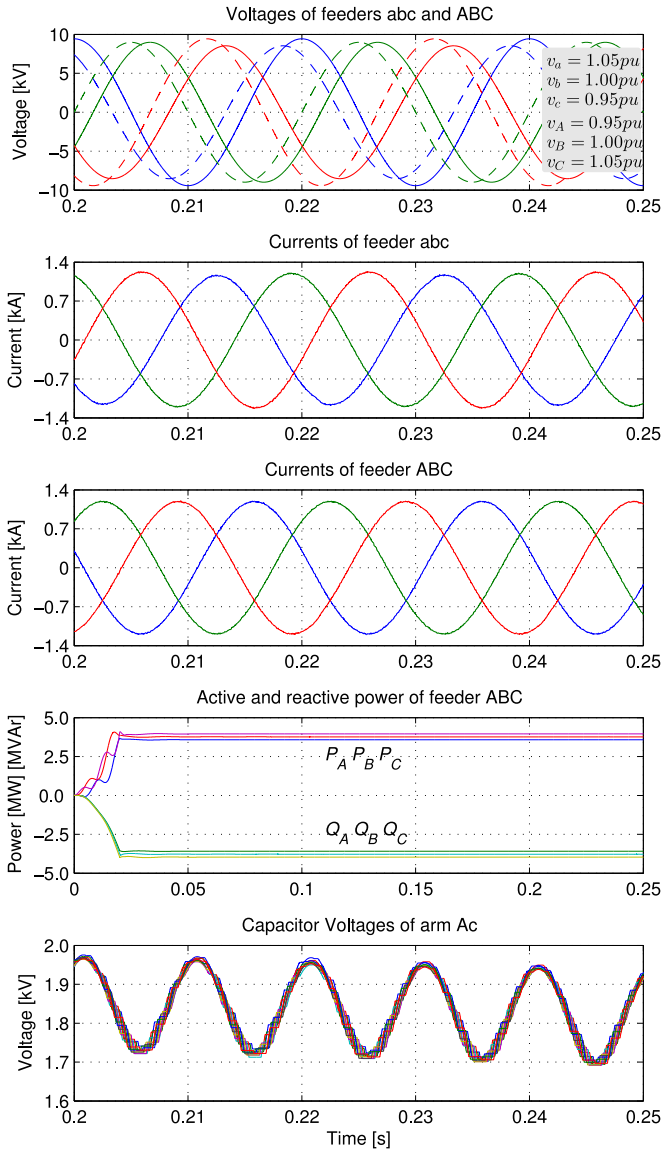


Fig. 10. Simulation results under worst conditions.

the converter is now 10 MVA because it is limited by the current of the feeder with lower voltage (6.6 kV). Fig. 11 shows the simulation results of the feeder voltages, the feeder currents, the voltage of arm Ac and the capacitor voltages of arm Ac. The THD of the line currents are 1.15% for the 11 kV feeder and 0.7% for the 6.6 kV feeder. The voltage generated by the arm has a lower voltage (fewer levels) than the previous simulations with two 11 kV feeders, because now the voltages among lines and the arm currents are lower, so the controller requires applying less voltage to control the converter. The capacitor voltages of arm Ac are balanced and have lower ripple for the same reason already given. It is important to notice that if there is a phase shift between the two feeders of different voltages, the direct MMC will generate different reactive powers in each feeder. Therefore, the reactive power of only one feeder can be controlled and the other one will be a function of the first one.

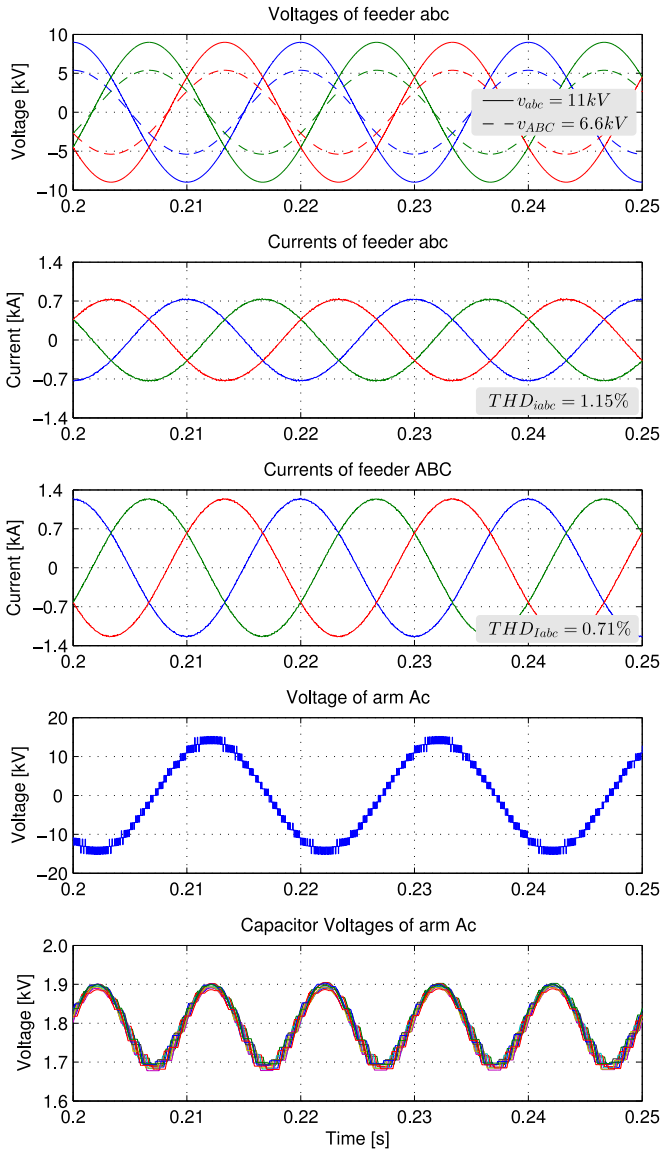


Fig. 11. Simulation results with systems with different nominal voltages.

V. Conclusion

The direct MMC is an ac-to-ac converter that combines some of the characteristics of the MMC and the matrix converters. The direct MMC uses full H-bridges connected in series, which means it generates more levels than the half-bridge MMC. As with other MMCs, it is highly modular and scalable to any power or voltage. It uses the same number of semiconductors as the back-to-back MMC, but it requires the half number of capacitors and coupling inductors because only six arms are necessary. The smaller number of modules, module capacitors and phase inductors may give the direct MMC a volume advantage over the B2B-MMC which is important in retrofitting to substations. However, the direct MMC has no dc-link and the currents in the two feeders are not independent.

The control of the direct MMC is simple and effective at any operation point, even at the worst case, when the voltages in the grid are highly unbalanced and the two feeders have a phase shift. However, the control parameters have to be chosen very carefully to achieve a good performance.

The current and voltage rating of the converter depends on the feeder voltages and phase shift, covering a wide range of possible values. However, in all practical cases the direct MMC requires lower blocking voltage but higher current rating than the B2B-MMC. Additionally, the direct MMC can be used between two feeders of different voltage (e.g., 11 kV – 6.6 kV) with some advantages over the B2B-MMC such as a considerably lower blocking voltage.

The current quality of the converter is high due to the large number of voltage levels generated (e.g., 21), so no filters are necessary, which increases the efficiency, especially at low power operation. Assuming an operation at rated power, unity power factor and without phase shift, the direct MMC has an efficiency of 97.54%, where the conduction losses represent 56% and the switching losses 44% if the frequency of the PS-PWM carrier is 400 Hz. The switching losses are practically the same as the B2B-MMC but the conduction losses are higher due to the higher current in each arm. However, the conduction losses are mitigated by the operation principle of the converter, which operates the current in quadrature with the voltage on each arm, reducing the average current that is carried by the IGBTs and increasing the current in anti-parallel diodes with somewhat lower conduction voltage. Then, the conduction losses are approximately 68% higher than the B2B-MMC.

The direct MMC converter shows a satisfactory performance and efficiency to be operated as a soft-open-point in MV systems under several scenarios. It presents advantages over the conventional back-to-back two-level inverter and the MMC, such as lower footprint and operation without filters. However, it has an important drawback, which is that the coupling of current between the two feeders entails a coupled reactive power between the two feeders and a limitation of the converter to assist only one feeder at a time when unbalance voltage or harmonic compensation is desired. There is scope for control and hardware development to solve these limitations in the future.

References

[1] M. Cavlovic, "Challenges of optimizing the integration of distributed generation into the distribution network," in *Proc. IEEE 8th Int. Conf. Eur. Energy Market*, May 2011, pp. 419–426.

[2] N. Saadat, S. S. Choi, and D. M. Vilathgamuwa, "A series-connected photovoltaic distributed generator capable of enhancing power quality," *IEEE Trans. Energy Convers.*, vol. 28, no. 4, pp. 1026–1035, Dec. 2013.

[3] M.-C. Alvarez-Herault, D. Picault, R. Caire, B. Raison, N. HadjSaid, and W. Bienia, "A novel hybrid network architecture to increase DG insertion in electrical distribution systems," *IEEE Trans. Power Syst.*, vol. 26, no. 2, pp. 905–914, May 2011.

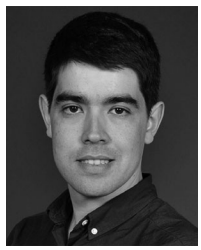
[4] W. A. Omran, M. Kazerani, and M. M. A. Salama, "Investigation of methods for reduction of power fluctuations generated from large grid-connected photovoltaic systems," *IEEE Trans. Energy Convers.*, vol. 26, no. 1, pp. 318–327, Mar. 2011.

[5] J. M. Bloemink and T. C. Green, "Increasing distributed generation penetration using soft normally-open points," in *Proc. IEEE Power Energy Soc. Gen. Meeting*, Jul. 2010, pp. 1–8.

[6] J. M. Bloemink and T. C. Green, "Increasing photovoltaic penetration with local energy storage and soft normally-open points," in *Proc. IEEE Power Energy Soc. Gen. Meeting*, Jul. 2011, pp. 1–8.

[7] A. Kechroud, J. M. A. Myrzik, and W. Kling, "Taking the experience from flexible AC transmission systems to flexible AC distribution systems," in *Proc. IEEE 42nd Int. Univ. Power Eng. Conf.*, Sep. 2007, pp. 687–692.

[8] J. M. Bloemink and T. C. Green, "Benefits of distribution-level power electronics for supporting distributed generation growth," *IEEE Trans. Power Del.*, vol. 28, no. 2, pp. 911–919, Apr. 2013.
[9] W. Cao, J. Wu, and N. Jenkins, "Feeder load balancing in MV distribution networks using soft normally-open points," in *Proc. IEEE Power Energy Soc. Innovat. Smart Grid Technol.*, Oct. 2014, pp. 1–6.
[10] M. Chiandone, G. Sulligoi, F. Milano, G. Piccoli, and P. Mania, "Back-to-back MVDC link for distribution system active connection: A network study," in *Proc. IEEE Int. Conf. Renew. Energy Res. Appl.*, Oct. 2014, pp. 1001–1006.
[11] S. Debnath, J. Qin, B. Bahrani, M. Saeedifard, and P. Barbosa, "Operation, control, and applications of the modular multilevel converter: A review," *IEEE Trans. Power Electron.*, vol. 30, no. 1, pp. 37–53, Jan. 2015.
[12] H. Akagi, M. Multilevel, C. Converter, and H. Akagi, "Classification, terminology, and application of the modular multilevel cascade converter (MMCC)," *IEEE Trans. Power Electron.*, vol. 26, no. 11, pp. 3119–3130, Nov. 2011.
[13] K. Sekiguchi, P. Khamphakdi, M. Hagiwara, and H. Akagi, "A grid-level high-power BTB (back-to-back) system using modular multilevel cascade converters withoutcommon DC-link capacitor," *IEEE Trans. Ind. Appl.*, vol. 50, no. 4, pp. 2648–2659, Jul./Aug. 2014.
[14] A. Nami, J. Liang, F. Dijkhuizen, and G. Demetriades, "Modular multilevel converters for HVDC applications: Reviewon converter cells and functionalities," *IEEE Trans. Power Electron.*, vol. 30, no. 1, pp. 18–36, Jan. 2015.
[15] P. Khamphakdi, K. Sekiguchi, M. Hagiwara, H. Akagi, S. Member, K. Sekiguchi, and M. Hagiwara, "A transformerless back-to-back (BTB) system using modular multilevel cascade converters for power distribution systems," *IEEE Tran. Power Electron.*, vol. 30, no. 4, pp. 1866–1875, Apr. 2015.
[16] S. Angkititrakul and R. Erickson, "Control and implementation of a new modular matrix converter," in *Proc. 19th Annu. IEEE Appl. Power Electron. Conf. Expo.*, 2004, no. C, pp. 813–819.
[17] R. Erickson, S. Angkititrakul, and K. Almazeedi, "A new family of multilevel matrix converters for wind power applications: final report," National Renewable Energy Laboratory (NREL), Denver, CO, U.S., Tech. Rep. NREL/SR-500-40051, Dec. 2006.
[18] A. J. Korn, M. Winkelnkemper, P. Steimer, and J. W. Kolar, "Direct modular multi-level converter for gearless low-speed drives," in *Proc. 14th Eur. Conf. Power Electron. Appl.*, 2011, pp. 1–7.
[19] W. Kawamura, M. Hagiwara, and H. Akagi, "Control and experiment of a modular multilevel cascade converter based on triple-star bridge cells (MMCC-TSBC)," *IEEE Trans. Ind. Appl.*, vol. XX, no. X, pp. 1–1, 2014.
[20] K. Ilves, L. Bessegato, and S. Norrga, "Comparison of cascaded multilevel converter topologies for AC/AC conversion," in *Proc. IEEE Int. Power Electron. Conf.*, May 2014, pp. 1087–1094.
[21] L. Baruschka and A. Mertens, "A new 3-phase direct modular multilevel converter," in *Proc. 14th Eur. Conf. Power Electron. Appl.*, 2011, vol. 2, no. 2, pp. 1–10.
[22] L. Baruschka and A. Mertens, "A new three-phase AC/AC modular multilevel converter with six branches in hexagonal configuration," *IEEE Trans. Ind. Appl.*, vol. 49, no. 3, pp. 1400–1410, May/Jun. 2013.
[23] R. Tsuruta, T. Hosaka, and H. Fujita, "A new power flow controller using six multilevel cascaded converters for distribution systems," in *Proc. IEEE Int. Power Electron. Conf.*, May 2014, pp. 1350–1356.
[24] M. Karimi-Ghartemani and M. Iravani, "A method for synchronization of power electronic converters in polluted and variable-frequency environments," *IEEE Trans. Power Syst.*, vol. 19, no. 3, pp. 1263–1270, Aug. 2004.
[25] CENELEC, "EN 62751-1: Power Losses in Voltage Sourced Converter (VSC) Valves for high-voltage direct current (HVDC) systems Part 1: General requirements," BSI, London, U.K, Tech. Rep. BS EN 62751-1:2014, 2014.
[26] CENELEC, "EN 62751-2: Power Losses in Voltage Sourced Converter (VSC) Valves for high-voltage direct current (HVDC) systems Part 2: Modular multilevel converters," BSI, London, U.K, Tech. Rep. BS EN 62751-2:2014, 2014.
[27] P. S. Jones and C. C. Davidson, "Calculation of power losses for MMC-based VSC HVDC stations," presented at the 15th Eur. Conf. Power Electron. Appl., EPE, Lille, France, 2013.
[28] The Electricity Council, "ENA ER P29: Planning Limits for Voltage Unbalance in the United Kingdom," The Electricity Council, London, U.K., Tech. Rep. BSD0989PDS, Mar. 1990.



Javier Pereda (S'09–M'14) received the B.Sc. (Eng.) (Hons.) degree in electrical engineering in 2009, and the M.Sc. and Ph.D. degrees in electrical engineering from Pontificia Universidad Católica de Chile, Santiago, Chile, in 2013.

He is an Assistant Professor in the Department of Electrical Engineering at Pontificia Universidad Católica de Chile since 2013 and an Associate Research of the Control and Power Group in the Electrical and Electronic Engineering Department at Imperial College London, London, U.K., since 2014. He is the Principal Investigator of the Electric Vehicle Laboratory and the Power and Energy Conversion Laboratory (PEClab) at Pontificia Universidad Católica de Chile. Currently, he is working on flexible distribution networks using power electronics to integrate distribution generation and electric vehicles. His research interests are power electronics and control for power conversion applied to electric vehicles, electric networks, renewable energy, industrial applications, and motor drives.



Tim C. Green (M'89–SM'02) received the B.Sc. (Eng.) (Hons.) degree in electrical engineering from Imperial College London, London, U.K., in 1986 and the Ph.D. degree in electrical engineering from Heriot-Watt University, Edinburgh, U.K., in 1990.

He is a Chartered Engineer in the U.K. He was a Lecturer at Heriot Watt University until 1994 and is now a Professor of Electrical Power Engineering at Imperial College London, Deputy Head of the Electrical and Electronic Engineering Department and Director of the Energy Futures Lab. His research interest is formulating the future from the electricity network to support low-carbon futures. A particular theme is how the flexibility of power electronics and control can be used to accommodate new generation patterns and new forms of load, such as electric-vehicle charging, as part of the emerging smart grid. He has particular interests in offshore dc networks and of management of low-voltage networks. He leads the HubNet consortium of eight UK universities coordinating research in low-carbon energy networks and is the Network Champion for the Research Councils U.K.